



Structure of a tripartite protein complex that targets toxins to the type VII secretion system

Timothy A. Klein^{a,b,1} , Prakhar Y. Shah^{a,b,1} , Polyniki Gkragakopoulou^{a,b}, Dirk W. Grebenc^{a,b} , Youngchang Kim^c , and John C. Whitney^{a,b,d,2}

Edited by Roy Curtiss III, University of Florida, Gainesville, FL; received July 20, 2023; accepted November 20, 2023

Type VII secretion systems are membrane-embedded nanomachines used by Gram-positive bacteria to export effector proteins from the cytoplasm to the extracellular environment. Many of these effectors are polymorphic toxins comprised of an N-terminal Leu-x-Gly (LXG) domain of unknown function and a C-terminal toxin domain that inhibits the growth of bacterial competitors. In recent work, it was shown that LXG effectors require two cognate Lap proteins for T7SS-dependent export. Here, we present the 2.6 Å structure of the LXG domain of the TelA toxin from the opportunistic pathogen *Streptococcus intermedius* in complex with both of its cognate Lap targeting factors. The structure reveals an elongated α -helical bundle within which each Lap protein makes extensive hydrophobic contacts with either end of the LXG domain. Remarkably, despite low overall sequence identity, we identify striking structural similarity between our LXG complex and PE-PPE heterodimers exported by the distantly related ESX type VII secretion systems of Mycobacteria implying a conserved mechanism of effector export among diverse Gram-positive bacteria. Overall, our findings demonstrate that LXG domains, in conjunction with their cognate Lap targeting factors, represent a tripartite secretion signal for a widespread family of T7SS toxins.

bacterial secretion systems | protein export | bacterial toxins | structural biology | protein biochemistry

The type VII secretion system (T7SS) is an integral membrane protein complex that facilitates the export of protein effectors through the cell envelope of Gram-positive bacteria. Likely owing to their distinct cell envelope architectures, bacteria belonging to the phyla Actinobacteria and Firmicutes encode distinct T7SS complexes referred to as T7SSa and T7SSb, respectively, with each subtype possessing several phylum-specific subunits (1). The ESX-1 T7SSa is well-studied in pathogenic Mycobacteria such as *Mycobacterium tuberculosis* because it is a major virulence factor required for the phagosomal escape step that precedes cytoplasmic replication of infected macrophages (2). Conversely, the T7SSb is less well understood but has recently been shown to play a role in both virulence and/or bacterial antagonism in both pathogenic and environmental bacteria (3–7).

The T7SSb is known to export two families of effector proteins. WXG100 proteins, which include the ubiquitous T7SS effector EsxA, are approximately 100 amino acid long α -helical proteins whose precise function is unclear but are unique in that they are required for overall T7SS apparatus function and are also secreted from the cell (8, 9). Besides these small non-enzymatic effectors, large multi-domain polymorphic toxins are also exported by several characterized T7SSb pathways with the best studied examples belonging to the LXG toxin family (4). LXG toxins contain a loosely conserved N-terminal leucine-x-glycine (LXG) domain from which the protein family derives its name and diverse C-terminal toxin domains (10). LXG toxins from several T7SSb-expressing bacteria including *Bacillus subtilis*, *Staphylococcus aureus*, *Enterococcus faecalis*, and *Streptococcus intermedius* have been identified and in most instances, the toxin domains have been shown to possess antibacterial activities that mediate bacterial antagonism (4–6, 11). While recent work has advanced our mechanistic understanding of how some of these toxins inhibit bacterial growth, less is known about the role of their N-terminal LXG domains (3, 4, 11). These domains have long been hypothesized to target effectors to the membrane-embedded T7SSb apparatus, however, this has yet to be shown experimentally (10).

Although the function of the LXG domain is incompletely understood, our group recently demonstrated that some of the toxins harboring these domains require so-called targeting factors for their export (12). These targeting factors, termed LXG-associated α -helical proteins 1 and 2 (Lap1 and Lap2), directly interact with LXG domains and are necessary for LXG toxin export. As is often the case for bacterial gene products that physically interact, *lap* genes co-occur with the gene encoding their cognate LXG toxin and are typically found upstream of the toxin gene. Lap targeting factors are small α -helical proteins that are structurally reminiscent of WXG100 effectors. Interestingly, Lap1

Significance

Many species of bacteria secrete protein toxins that target eukaryotic and/or prokaryotic cells. In Gram-positive bacteria, one of the ways toxins are exported from cells is by a membrane protein complex known as the type VII secretion system. The mechanism by which one of the major families of toxins transits this pathway has remained unknown. Using biochemical and structural approaches, this study demonstrates that a conserved N-terminal domain found in this widespread toxin family functions as an export signal that targets toxins to the secretion apparatus. Overall, our findings represent a new mechanism of protein export and provide fundamental unique insight into how bacteria target toxins to competitor and host cells.

Author affiliations: ^aMichael DeGroot Institute for Infectious Disease Research, McMaster University, Hamilton, ON L8S 4K1, Canada; ^bDepartment of Biochemistry and Biomedical Sciences, McMaster University, Hamilton, ON L8S 4K1, Canada; ^cStructural Biology Center, X-ray Science Division, Advanced Photon Source, Argonne National Laboratory, Lemont, IL 60439; and ^dDavid Braley Centre for Antibiotic Discovery, McMaster University, Hamilton, ON L8S 4K1, Canada

Author contributions: T.A.K., P.Y.S., and J.C.W. designed research; T.A.K., P.Y.S., P.G., D.W.G., and Y.K. performed research; T.A.K., P.Y.S., and Y.K. analyzed data; and T.A.K., P.Y.S., and J.C.W. wrote the paper.

The authors declare no competing interest.

This article is a PNAS Direct Submission.

Copyright © 2024 the Author(s). Published by PNAS. This article is distributed under [Creative Commons Attribution-NonCommercial-NoDerivatives License 4.0 \(CC BY-NC-ND\)](https://creativecommons.org/licenses/by-nc-nd/4.0/).

¹T.A.K. and P.Y.S. contributed equally to this work.

²To whom correspondence may be addressed. Email: jwhitney@mcmaster.ca.

This article contains supporting information online at <https://www.pnas.org/lookup/suppl/doi:10.1073/pnas.2312455121/-DCSupplemental>.

Published January 9, 2024.

proteins possess a conserved FxxxD motif similar to the YxxxD/E export motif of T7SSa effectors (13, 14). Furthermore, mutation of this motif in the LapD1 targeting factor abrogates secretion of its cognate LXG toxin, TelD (12).

In the present study, we identify two additional families of targeting factors, termed Lap3 and Lap4, and show that members of these families found upstream of the *S. intermedius* LXG-containing toxin TelA are required for effector secretion. Using X-ray crystallography, we solve the structure of these targeting factors in complex with the LXG domain of TelA, revealing the molecular basis of how LXG domains simultaneously interact with both of their targeting factors. Using TelA as a model, we subsequently show that the LXG domain is both necessary and sufficient for protein export by the T7SSb and identify key amino acid motifs involved in this process. Finally, using AlphaFold2 models informed by our structure, we provide evidence that diverse LXG toxin complexes adopt a conserved tripartite architecture at their N-terminus that is required for their secretion by the T7SSb.

Results

Identification of Two New Families of LXG Toxin Targeting Factors. While many LXG toxins are encoded downstream of a Lap1–Lap2 pair (formerly DUF3130–DUF3958), others are found downstream of DUF5344 and DUF5082 encoding genes, which are also predicted to encode for small α -helical proteins (SI Appendix, Fig. S1) (8). The opportunistic pathogen *Streptococcus intermedius* B196 (Si^{B196}) has a single *lap1*–*lap2* associated effector, TelC, and two DUF5344–DUF5082 associated effectors, TelA and TelB (Fig. 1A). Because of their genetic association with LXG effectors and their predicted α -helical secondary structure,

we henceforth refer to DUF5344–DUF5082 pairs as Lap3 and Lap4 to reflect their predicted similarity to Lap1 and Lap2, respectively (SI Appendix, Fig. S1). This similarity also led us to hypothesize that like *lap1* and *lap2* deletion strains, strains lacking either *lap3* or *lap4* would be unable to export their downstream effector. To test this prediction, we focused on the TelA toxin and its corresponding Lap proteins, LapA3 and LapA4, to examine the role of these uncharacterized protein families in LXG toxin export. In line with our hypothesis, Si^{B196} strains bearing inactivating mutations in either *lapA3* or *lapA4* fail to export TelA and this secretion defect could be restored through plasmid-borne expression of the deleted *lap* genes in the corresponding deletion strains (Fig. 1B).

The *telA* and *telB* gene neighborhoods possess an additional gene that encodes for a member of the DUF4176 family of uncharacterized proteins, which are absent in the *telC* gene cluster (Fig. 1A). To test the potential involvement of DUF4176 proteins in LXG toxin secretion, we generated a strain lacking the DUF4176 encoding gene upstream of *telA*, SIR_0168, and again assayed for TelA export. As is the case for *lapA3* and *lapA4* deficient strains of Si^{B196}, TelA is not secreted by a strain lacking SIR_0168 and secretion could be restored by trans complementation of SIR_0168 (Fig. 1B).

We next wanted to test whether the protein product of each gene required for TelA secretion is exported from cells. We and others previously found that the targeting factors for TelC toxins, LapC1 and LapC2, are not secreted from cells (12, 15). To test whether this is also the case for LapA3 and LapA4, we expressed C-terminal VSV-G tagged versions of these proteins and performed western blot analyses on cell and culture supernatant fractions of wild-type and T7SS-null (Δ *essC*) strains of Si^{B196}. In contrast to LapC1 and LapC2, we could readily detect T7SSb-dependent export of LapA3

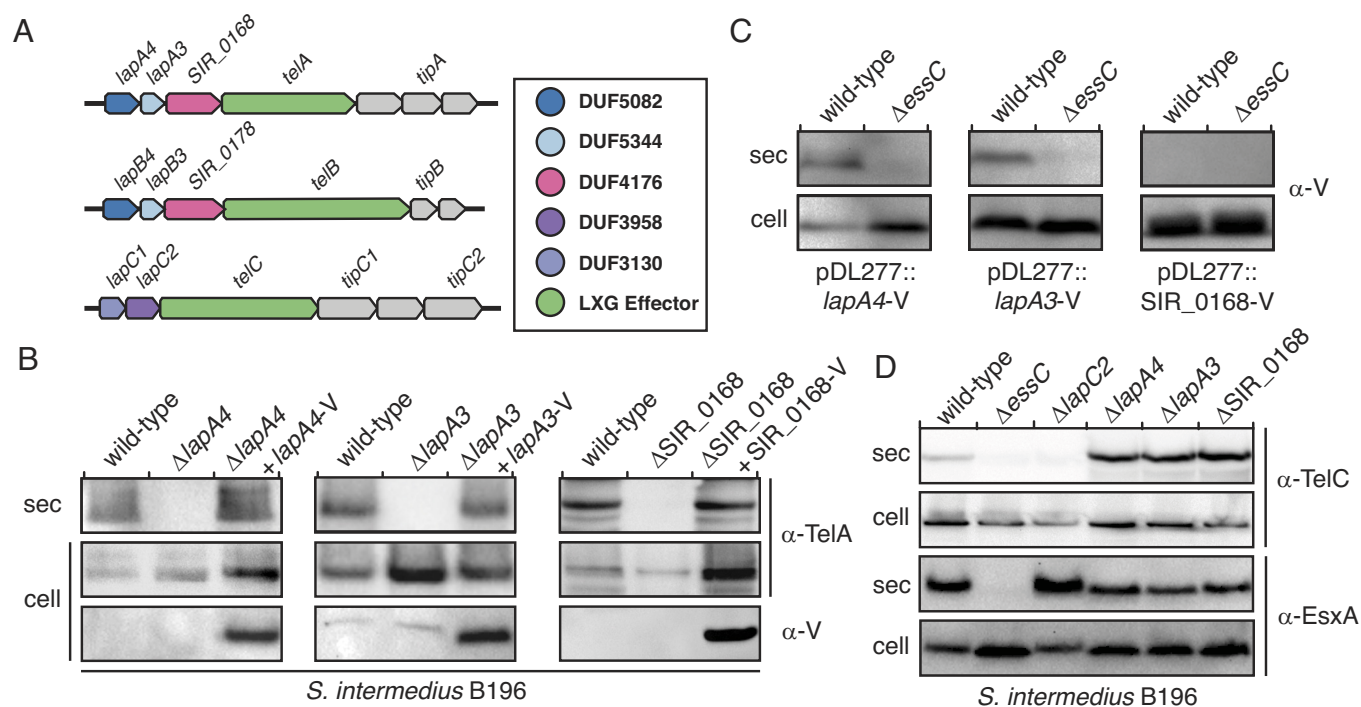


Fig. 1. TelA toxin is co-secreted with its cognate targeting factors. (A) Genomic context of the genes encoding the three Tel toxins exported by the T7SS of *S. intermedius* B196, their cognate Tip immunity proteins that protect against intra- and intercellular intoxication, and Lap targeting factors. (B) Western blot showing that *lapA4*, *lapA3*, and *SIR_0168* are required for the secretion of TelA toxin. For each blot, TelA secretion (sec) is compared between wild-type *S. intermedius* B196, the indicated deletion mutant, and the deletion mutant complemented with plasmid-borne expression of the deleted gene harboring a C-terminal VSV-G (V) epitope tag to facilitate its detection by western blot. (C) LapA4 and LapA3 are exported from cells in a T7SS-dependent manner, whereas SIR_0168 is not. Western blots examining the secretion of the protein products of the indicated plasmid-borne genes expressed in either wild-type *S. intermedius* B196 or a strain lacking a functional T7SSb (Δ *essC*). (D) Lap targeting factors are specific for their cognate Tel toxin. Western blot analysis of EsxA and TelC secretion in *S. intermedius* B196 strains lacking *lapA4*, *lapA3*, or *SIR_0168*.

and LapA4 (Fig. 1C). We also found that the Lap3–Lap4 pair associated with the TelB LXG toxin, LapB3 and LapB4, are similarly secreted in a T7SSb-dependent manner (*SI Appendix, Fig. S2*). This difference in localization for the different Lap pairs suggests that Lap3 and Lap4 proteins may promote the secretion of their cognate effectors in a way that is mechanistically distinct from Lap1–Lap2. Finally, we also tested for secretion of VSV-G tagged SIR_0168 and found that this protein is not secreted by Si^{B196} indicating that despite being required for TelA secretion, it is likely not exported from cells alongside TelA, LapA3, and LapA4 (Fig. 1C).

WXG100 effectors such as EsxA are typically encoded next to genes encoding the T7SSb apparatus and based on structural studies of T7SSa systems are likely involved in the export of all T7SS effectors due to their role in the formation of an active T7SS apparatus pore (16–18). By contrast, each *tel* gene in the Si^{B196} genome is found adjacent to a unique set of *lap* genes. This observation led us to hypothesize that Lap proteins are highly specific and are therefore likely only required for the secretion of their cognate effector. To test this, we used a TelC-specific antibody to assay for cellular and secreted levels of TelC in our *lapA3*, *lapA4*, and SIR_0168-deficient strains. The deletion of any of the three genes required for TelA secretion had no effect on extracellular levels of TelC, whereas a strain lacking the LapC2 targeting factor was unable to export TelC (Fig. 1D). Taken together, these data indicate that the targeting factors encoded upstream of LXG genes are indeed effector-specific and are therefore not required for global T7SS effector export.

Structure of the TelA_{LXG}–LapA3–LapA4 Complex. To better understand the function of LXG domains and their potential interactions with Lap targeting factors, we next sought to determine

their three-dimensional structures by X-ray crystallography. We previously showed that TelC, LapC1, and LapC2 physically interact to form a heteromeric complex, however, crystallization of this particle proved refractory (12). Therefore, we adopted a similar co-expression and co-purification strategy with the LXG domain of TelA (residues 1–224) or TelB (residues 1–219) along with their cognate targeting factors and found that like TelC they interact to form a 1:1:1 complex (Fig. 2A and *SI Appendix, Fig. S3 A and B*). Of these two complexes, TelA_{LXG}–LapA3–LapA4 crystallized readily, and we were able to solve its crystal structure to a resolution of 2.6 Å using molecular replacement with an AlphaFold2 generated model of the trimeric complex as a search model (Table 1).

The overall structure of TelA_{LXG}–LapA3–LapA4 reveals that the complex formed by these proteins forms an elongated α -helical bundle with approximate dimensions of ~ 180 Å by ~ 30 Å (Fig. 2B). Within this bundle structure, LapA3 and LapA4 both adopt a helix-turn-helix topology with the α -helices of the former aligning approximately parallel to one another, whereas those of the latter cross over at the protein's termini. TelA_{LXG} is composed of nine α -helices that are divided into two sub-domains by a central region containing two short antiparallel β -strands (Fig. 2C). Each of these sub-domains interacts with a single Lap protein with one sub-domain consisting of α -helices 4–6 and interacting with LapA4 and the other comprising α -helices 1–3 and 7–9 and interacting with LapA3. Remarkably, despite the relatively small size of each of the subunits within this complex, the buried surface areas between TelA_{LXG}–LapA3 and TelA_{LXG}–LapA4 are 2,261.5 Å² and 1,810.4 Å², respectively. Analysis of the surface properties of these interfaces reveals that they are highly hydrophobic in nature suggesting that complex formation is largely entropically driven (Fig. 2D).

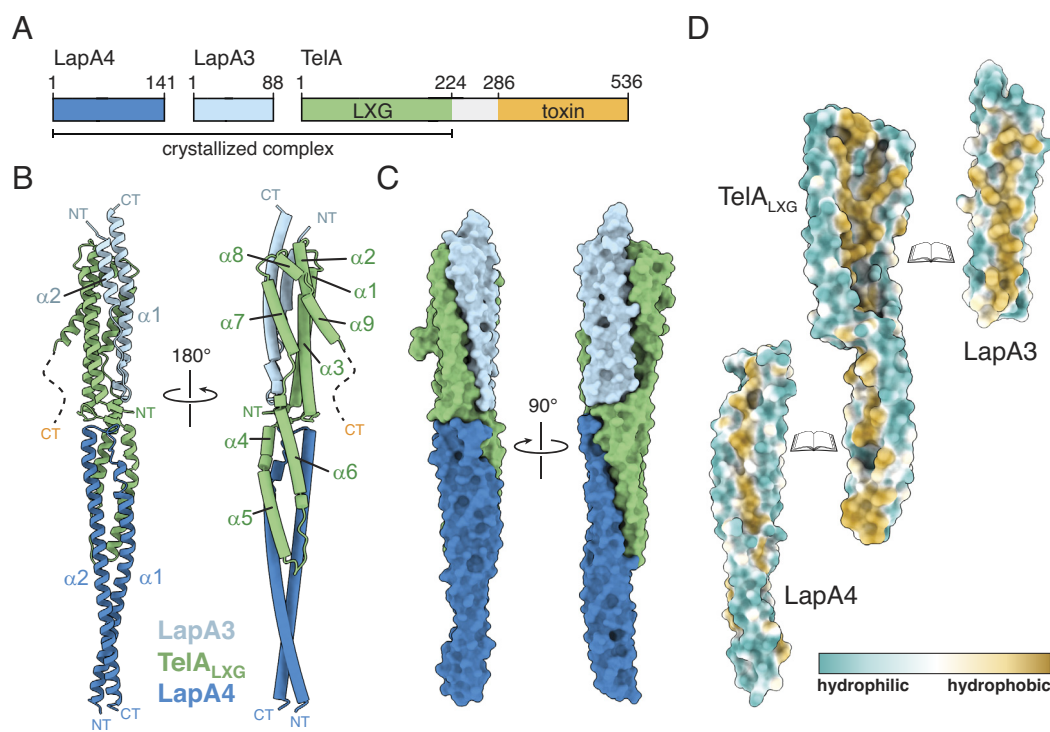


Fig. 2. Overall structure of the TelA_{LXG}–LapA4–LapA3 complex. (A) Domain schematic of LapA4, LapA3, and TelA depicting the amino acid boundaries of the crystallized complex. (B) Cartoon model of the TelA_{LXG}–LapA4–LapA3 complex shown from two opposing views colored in green, dark blue, and light blue, respectively. The secondary structure elements and termini of each protein subunit are indicated. The approximate location of TelA's middle region (residues 224–286) and C-terminal toxin domain (CT) is indicated by a dashed line. (C) Space-filling model of the TelA_{LXG}–LapA4–LapA3 complex shown from two orthogonal angles. (D) Hydrophobic surface representation depicting the interaction interfaces between TelA_{LXG} and each of its Lap targeting factors.

Table 1. X-ray data collection and refinement statistics

| TelA_1-223:LapA3:LapA4 (native) | |
|--|------------------------|
| Data Collection | |
| Wavelength (Å) | 0.97918 |
| Space group | P1 |
| Cell dimensions | |
| <i>a</i> , <i>b</i> , <i>c</i> (Å) | 51.9, 61.4, 97.9 |
| α , β , γ (°) | 77.7, 77.1, 65.1 |
| Resolution* (Å) | 45.08–2.60 (2.64–2.60) |
| Unique reflections | 31,528 (1,504) |
| CC _{1/2} [†] | 0.948 (0.478) |
| <i>R</i> _{merge} [‡] | 0.209 (0.858) |
| <i>R</i> _{pim} [‡] | 0.123 (0.586) |
| <i>I</i> / σ <i>I</i> | 7.9 (1.0) |
| Completeness (%) | 97.2 (92.9) |
| Redundancy | 3.7 (2.7) |
| Wilson B-factor | 41.5 |
| Refinement | |
| <i>R</i> _{work} [§] / <i>R</i> _{free} (%) | 21.5/25.8 |
| Average B-factors (Å ²) | |
| Protein | 56.2 |
| Water/Other | 47.5/60.9 |
| No. atoms | |
| Protein | 6614 |
| Water/Other | 275/12 |
| Rms deviations | |
| Bond lengths (Å) | 0.001 |
| Bond angles (°) | 0.300 |
| Ramachandran plot (%) | |
| Total favored [¶] | 98.84 |
| Total allowed | 1.16 |
| PDB code | 8GMH |

*Values in parentheses correspond to the highest resolution shell.

[†]As defined by Karplus and Diederichs (19).

[‡] $R_{\text{merge}} = \frac{\sum_i \sum_j |I_{ij} - \langle I_i \rangle|}{\sum_i \sum_j I_{ij}}$, where I_{ij} is the intensity of observation *j* of reflection *i*.

[§] $R = \frac{\sum_i |F_o - F_c|}{\sum_i |F_o|}$ for all reflections, where F_o and F_c are observed and calculated structure factors, respectively. *R*_{free} is calculated analogously for the test reflections, randomly selected, and excluded from the refinement.

[¶]As defined by MolProbity (20).

The TelA_{LXG} and LapA3 Subcomplex Resembles Substrates of Mtb ESX T7SSs. Upon initial inspection of the TelA_{LXG}–LapA3–LapA4 structure, it was immediately apparent that it possesses many similarities to structurally characterized T7SSa effectors including EspB and the PE25–PPE41 heterodimer exported by the ESX-1 and ESX-5 systems of *M. tuberculosis*, respectively (Fig. 3A) (14, 21). EspB and PE25–PPE41 heterodimers adopt similar all α -helical folds with the former resembling a fused version of the latter. These two T7SSa effectors share a similar shape and topology with the TelA_{LXG} and LapA3 components of our T7SSb effector complex. Unlike TelA, EspB, and PE25–PPE41 do not harbor C-terminal toxin domains and instead are proposed to oligomerize into pores in the outer membrane of *M. tuberculosis* (22, 23). Given that T7SSb-containing Firmicutes lack an outer membrane, it is perhaps not surprising that we observe no such oligomeric arrangement for TelA_{LXG}–LapA3–LapA4 in the crystal lattice of our structure.

We next used multiple sequence alignments to search for conserved motifs within TelA_{LXG}, LapA3, and LapA4 to identify residues that are likely important for function. Not surprisingly, given our prior analyses of TelC_{LXG}, Lap1, and Lap2 sequences, we found that these proteins contain little overall sequence conservation (12). Nonetheless, two prominent motifs emerged from our analysis with the first being TelA's LxG motif from which LXG toxins derive their name and the second being an NKxxDD motif found at the C-terminus of LapA3 (Fig. 3A). Interestingly, these motifs are found near one another in three-dimensional space and bear a striking resemblance to the well-characterized export arm motif of T7SSa substrates (13, 14, 24). For example, Leu41 of the LxG motif is found in the same turn region of TelA as is the conserved WxG motif of PPE41. In both proteins, the conserved hydrophobic residue in these motifs is buried in a hydrophobic pocket of its interacting partner to buttress its solvent-exposed C-terminal α -helix. The second motif is less well conserved between T7SSa and T7SSb substrates in that the tyrosine residue found in the YxxxD/E export arm motif of EspB and PE25 is absent in LapA3 (13, 14). Nevertheless, all three proteins possess the conserved solvent-exposed acidic residue within this motif in approximately the same position in their structure with LapA3 uniquely possessing two aspartic acid residues at this site (Fig. 3B). Given the importance of residues in this position for type VII secretion, we mutated each conserved aspartic acid residue of LapA3 to alanine and examined the ability of these variants to facilitate TelA secretion. In line with their high degree of sequence conservation, expression of the D79A variant resulted in a substantial reduction in TelA secretion whereas the levels of secreted TelA in cells expressing the D80A variant were reduced to that of the Δ lapA3 negative control (Fig. 3C). When taken together with mutagenesis analysis of other T7SS substrates, these data indicate that a conserved C-terminal acidic residue appears to be a universal requirement for protein export by the T7SS apparatus (9, 12, 13).

LXG Complexes Target Toxins for Export by the T7SSb. Our data so far suggest that LXG–Lap–Lap heterotrimeric complexes represent a tripartite trafficking complex that targets LXG toxins for T7SSb-dependent export from the cell. To test this hypothesis, we first examined the ability of TelC to be exported from cells in the absence of its LXG domain (TelC _{Δ LXG}). We chose TelC for this initial experiment because our antibody for this protein recognizes its toxin domain, whereas our TelA antibody recognizes TelA's LXG domain. In line with our prediction, we found that in contrast to full-length TelC, which is readily exported from cells, TelC _{Δ LXG} remains in the cytoplasm (Fig. 3D). We next sought to examine whether LXG complexes are sufficient for T7SSb-dependent protein export. To test this, we employed a recently developed split luciferase assay in which an 11 amino acid fragment of deep-sea shrimp luciferase is fused to a protein of interest and that protein's export is assessed by measuring the ability of the fused fragment to combine with the remainder of the luciferase enzyme added exogenously via its bioluminescence activity (25). After confirming the suitability of this assay for use in *S.*^{B196} using EsxA export as a positive control, we fused the luciferase fragment to the LXG domains of TelA and TelC, co-expressed these domains with their cognate Lap proteins and measured whether these heterotrimeric complexes are sufficient for protein export via the T7SSb. Consistent with functioning as a T7SSb targeting complex, we could detect TelA and TelC LXG domain export despite these proteins lacking their C-terminal toxin domains (Fig. 3E). By contrast, we did not detect secretion of TelC's toxin domain (TelC_{tox}) even though our

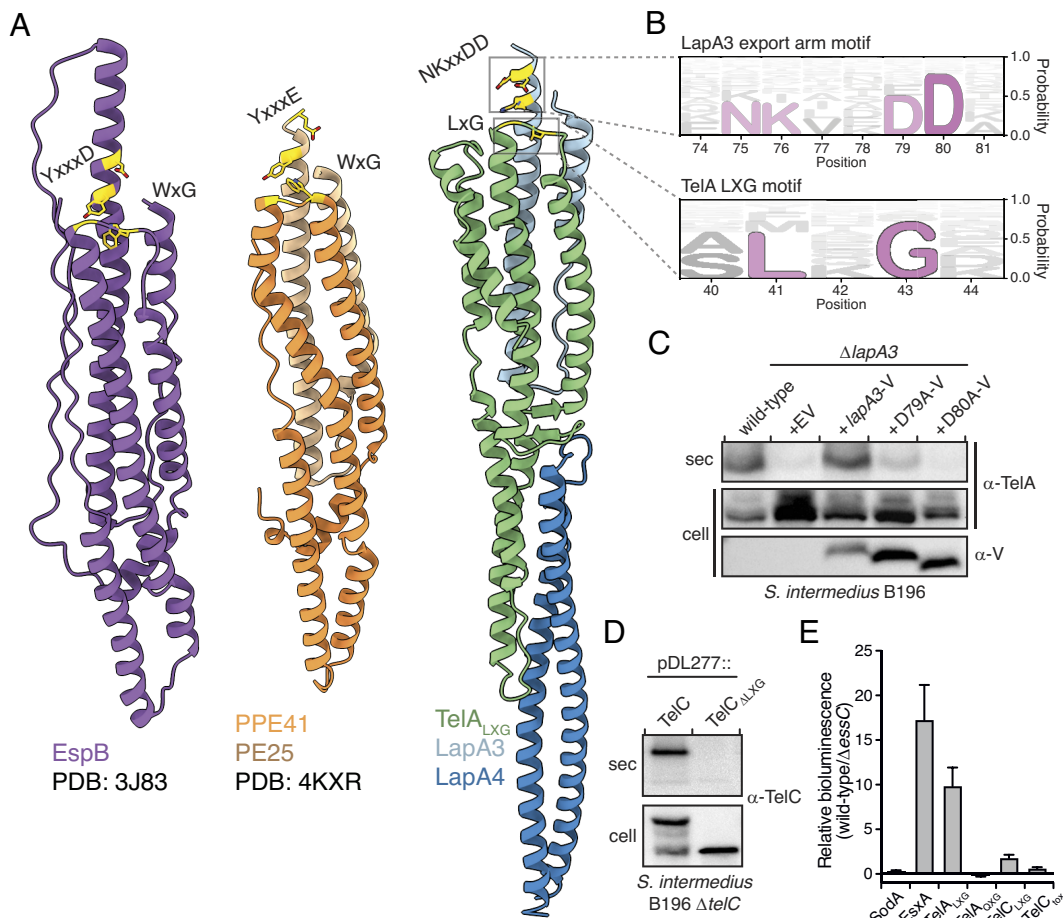


Fig. 3. LXC complexes are necessary and sufficient for T7SSb toxin export. (A) Structural comparison between $TelA_{LXC}$ -LapA4-LapA3 complex and the well-characterized T7SSa substrates EspB (PDB code 3J83) and PE25-PPE41 (PDB code 4KXR) from *M. tuberculosis*. Regions highlighted yellow indicated the residues comprising the conserved export arm in the *M. tuberculosis* substrates and the comparable residues in TelA and LapA3. (B) Sequence logo representation illustrating the conservation of the export arm and LXC motifs of LapA3 and TelA, respectively. Pink letters indicate the most conserved residues found in LapA3 and TelA homologous proteins. (C) Conserved LapA3 export arm motif residues are required for TelA toxin secretion from *S. intermedium* B196. Western blot analysis of TelA secretion (sec) in wild-type *S. intermedium* B196, a $\Delta lapA3$ mutant, and a $\Delta lapA3$ mutant complemented with C-terminal VSV-G epitope-tagged LapA3 (LapA3-V) and the indicated LapA3-V site-specific variants. (D) The LXC domain of TelC is required for its export via the T7SSb. Western blot analysis of the cell and secreted (sec) fractions of *S. intermedium* B196 strains expressing full-length TelC or TelC lacking its N-terminal LXC domain (TelC $_{\Delta LXC}$). (E) LXC domains of Tel effectors along with their cognate Lap proteins are sufficient for type VII secretion. Split nanoluciferase assay in which the indicated proteins were fused to the small subunit of nanoluciferase and the bioluminescence of culture supernatants containing purified nanoluciferase large subunit was measured. Superoxide dismutase (SodA) was used as a cytoplasmic protein control. For additional details, see *Experimental Procedures*.

prior work showed that this isolated domain is properly folded and enzymatically active (26). The extremely cytotoxic nature of TelA's toxin domain precluded a similar analysis of this Tel toxin (4). We next tested the functional importance of the conserved leucine residue that comprises the LXC motif by making a single amino acid substitution to glutamine in $TelA_{LXC}$ ($TelA_{QXC}$). In line with playing a critical role in the export process, we were unable to detect luminescence from the culture supernatant of a strain expressing $TelA_{QXC}$ heterotrimeric complexes. Importantly, SDS-PAGE and circular dichroism spectroscopy analyses of purified $TelA_{QXC}$ -LapA3-LapA4 complex demonstrate that this mutation does not affect complex formation or grossly perturb its overall secondary structure, and therefore instead likely plays a role in targeting TelA to the T7SSb apparatus (*SI Appendix, Fig. S3 C and D*). Collectively, these data indicate that LXC-domain containing complexes are both necessary and sufficient for type VIIb secretion.

LXC Targeting Complexes Adopt a Conserved Architecture.

While the structure and function of TelA's toxin domain are unknown and its AlphaFold2 predicted structure is low confidence,

we reasoned that we could use our experimental structure of $TelA_{LXC}$ -LapA3-LapA4 to predict the structure of other full-length LXC toxins for which the structure of the toxin has been determined or is confidently predicted (Fig. 4). Like TelA, we found AF2 predictions of TelB to be low confidence likely owing to the presence of a long linker region connecting its N-terminal LXC domain to its C-terminal toxin domain (4). By contrast, we were able to generate high-confidence models of full-length TelC because an X-ray structure is available for its toxin domain and of full-length YxiD toxin from *B. subtilis* because it lacks a middle linker region and possesses a confidently predicted nuclease toxin (4, 5). Based on these results and preliminary structural data described by others, we propose that full-length toxin-Lap-Lap complexes adopt a tomahawk-shaped structure with the metaphorical blade and shaft subunits being formed by the toxin domain and LXC-Lap-Lap complex, respectively (27). Given that there are currently over 4000 annotated LXC toxins in publicly available sequence databases, we expect that our structure will allow for the high-confidence modeling of the vast majority of tripartite LXC secretion complexes found in diverse species of T7SS-containing Firmicutes.

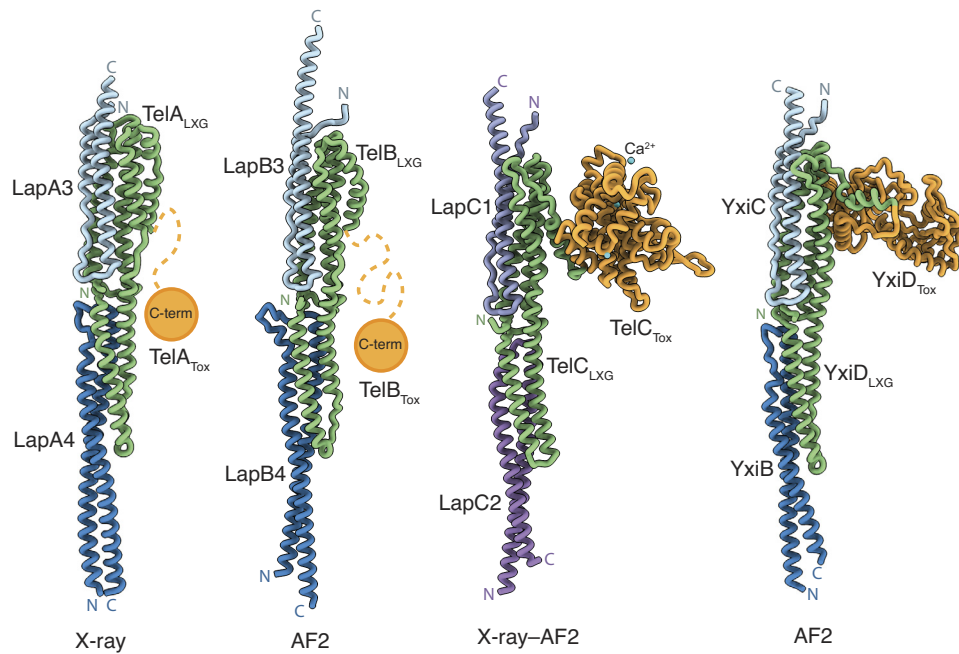


Fig. 4. LXG toxin complexes adopt a conserved tripartite architecture at their N-terminus and harbor diverse C-terminal toxin domains. Experimental and AlphaFold2 predicted structures of LXG toxins and their cognate Lap targeting factors. Low-confidence toxin domains are depicted as orange circles (TelA and TelB), whereas experimentally determined (TelC_{tox}, PDB code 5UKH) and high-confidence toxin domains (YxiD_{tox} from *B. subtilis*) are shown as orange ribbons.

Discussion

In this study, we have determined the first structure of an LXG domain and demonstrated that it represents the minimum requirement for LXG effector export by the T7SSb apparatus. In addition, we find that targeting factors belonging to the DUF5082 and DUF5344 protein families are co-exported as part of an N-terminal toxin trafficking complex required for type VIIb secretion. Given the widespread distribution of these protein families among Firmicutes, we anticipate our findings will be broadly applicable to LXG toxins from diverse bacterial species.

While our work defines the minimal requirement for type VIIb secretion, in some instances, additional cellular factors are required for LXG toxin export. For example, we found that TelA export also requires the DUF4176 family member, SIR_0168. While SIR_0168 itself is not secreted from cells, we speculate that it may function as a cytosolic chaperone that maintains TelA–LapA3–LapA4 complexes in a secretion-competent state, perhaps in a manner that is analogous to EspG proteins from T7SSa systems (21, 28). However, it is unclear why some effectors require a DUF4176 protein whereas others do not. One possibility is that LXG toxins with an extended middle domain between their LXG and toxin domains, like TelA and TelB, require a DUF4176 protein for intracellular trafficking whereas those that lack this middle domain, like TelC, do not (4). The site of action of the TelA and TelB toxins is in the cytoplasm of competitor bacteria whereas TelC acts extracellularly. Therefore, one tantalizing possibility is that the middle domain is involved in toxin translocation across the membrane of target cells and that the function of DUF4176 proteins in toxin-producing cells is to prevent erroneous membrane insertion prior to toxin export via the T7SSb.

The asymmetric structural models of LXG–Lap–Lap complexes raise interesting questions regarding the folded state of LXG toxins as they translocate the T7SSb apparatus. While recent cryo-electron microscopy structures of the ESX-1 and ESX-5 T7SSa apparatuses

show the closed conformation of the EccC/EssC translocase, estimates of the dimensions of the open complex based on structural comparisons to the related ATPase FtsK suggest its diameter is approximately 30 Å, which closely matches that of the N-terminal shaft complex composed of the LXG domain and its two cognate targeting factors (17, 18, 29, 30). This observation leads us to speculate that the C-terminal toxin domains likely exist in an unfolded state as they transit the T7SSb apparatus. Otherwise, their asymmetric shape would not be conducive to export through the symmetrical pore of the T7SS apparatus because doing so would likely compromise essential ion gradients required for cellular viability. Furthermore, the toxin domain unfolding prior to export would also provide a plausible mechanism for immunity protein dissociation in toxin-producing bacteria.

Another outstanding question that remains is how LXG toxin complexes are specifically recognized by the T7SSb apparatus. A likely candidate to fulfill this role is a C-terminal region of EssC that consists of a portion of its second ATPase domain and the entirety of its third ATPase domain (31, 32). In contrast to the rest of the T7SSb apparatus components, several bioinformatic studies show that the amino acid sequence of this region of EssC varies significantly even between strains of the same bacterium and likely coevolved with a suite of cognate LXG toxins (31, 33). While our attempts to observe a physical interaction between purified Tel pre-secretion complexes and various regions of EssC have thus far been met with limited success, this is perhaps not surprising as it remains unclear how the conformational states of the EssC translocon are regulated and such regulatory inputs may be needed before EssC and LXG toxin complexes can physically interact. Based on studies of T7SSa systems, these inputs likely include interaction with other components of the T7SSb apparatus, EsxA-induced multimerization, and ATP hydrolysis by the ATPase domains of EssC (16, 18). Future investigations into the specific roles that each of these components plays in the export process will be critical to furthering our understanding of the molecular mechanism of type VII effector secretion.

Experimental Procedures

Bacterial Strains, Plasmids, and Growth Conditions. All gene knockouts were introduced into a *S. intermedii* B196 wild-type background and genomic DNA from this organism was used as a PCR template for all molecular cloning. *E. coli* XL1-Blue and BL21 (DE3) CodonPlus were used for molecular cloning and protein overexpression, respectively. The complete list of bacterial strains used in this study is listed in *SI Appendix, Table S1*. pET29b- and pETDuet-1-derived plasmids were used for recombinant protein expression in *E. coli*, while pDL277-derived plasmids were used for constitutive protein expression in *S. intermedii*. PCR amplification of *S. intermedii* genes was done with Phusion polymerase (NEB). PCR amplicons were digested with NcoI/SalI for pETDuet-1 MCS1, NdeI/XhoI for pET29b/pETDuet-1 MCS2, or BamHI/SalI for pDL277 and the genes of interest were ligated into the respective plasmids with T4 DNA ligase (NEB). Additionally, some primers included an additional 3' sequence to generate tagged proteins with poly-6-His (HHHHHH), VSV-G (YTDIEMNRLGK), or GSG-linker-pep86 (GSGVSGWRLFKKIS) for protein purification, western blot detection, or nano-luciferase-based secretion assays, respectively. When cloning into pDL277, the P96 promoter sequence described by Lo Sapio and colleagues from *Streptococcus pneumoniae* was fused upstream to the gene of interest using splicing by overlap extension (SOE) PCR (34). A comprehensive list of the plasmids used in this study are found in *SI Appendix, Table S2*. *E. coli* was grown in lysogeny broth at 37 °C at 225 rpm under aerobic conditions. The growth media was supplemented with 50 µL/mL of kanamycin, 150 µL/mL of carbenicillin, or 100 µL/mL spectinomycin to select for pET29b, pETDuet-1, or pDL277, respectively. *S. intermedii* was grown in Todd Hewitt broth supplemented with 0.5% yeast extract (THY) in a 37 °C stationary 5% CO₂ incubator. All *S. intermedii* strains were grown on THY agar plates for 1 to 3 d prior to growth in THY broth to ensure uniform growth rate. THY broth and agar plates were supplemented with 250 µL/mL of kanamycin or 75 µL/mL of spectinomycin to select for gene deletions and pDL277-derived plasmids, respectively.

DNA Manipulation. To prepare genomic DNA, *S. intermedii* overnight cultures were pelleted and resuspended in a 10:1 ratio of culture to InstaGene Matrix (BioRad) after which the extraction protocol as per the manufacturer's instructions was followed. The DNA primers used in this study were generated by Integrated DNA Technology (IDT). Molecular cloning was done using Phusion polymerase, common restriction endonucleases, and T4 DNA ligase from NEB. Sanger sequencing was performed by Azenta Life Sciences and The Center for Applied Genomics at The Hospital for Sick Children in Toronto, Ontario.

Transformation of *S. intermedii*. Linear DNA fragments for allelic replacement (see below) or pDL277-derived plasmids were transformed into *S. intermedii* as previously described (35). In brief, *S. intermedii* overnight cultures were back diluted 1:10 into 2 mL THY broth supplemented with 5 µL of 0.1 mg/mL *S. intermedii* competence stimulating peptide (DSRIRMGFDFSKLFGK, synthesized by Genscript) and incubated for 2 h at the appropriate growth conditions (see above). Then, 100 to 200 ng of linear or plasmid DNA was then added, and cultures were grown for an additional 3 h before plating on THY agar plates supplemented with the appropriate antibiotic.

Gene Deletion in *S. intermedii* by Allelic Exchange. *S. intermedii* gene deletions were performed as described previously (36). In short, gene deletion constructs were assembled in pETDuet-1

plasmid using SOE PCR. These constructs were composed of 1,000 bps upstream of the gene of interest (5' flank) including the first 15 to 45 bps of the gene of interest ORF, a spectinomycin promoter derived from pDL277, a kanamycin resistance cassette from pBAV1K, and 1,000 bps downstream of the gene of interest (3' flank) including the last 15 to 45 bps of the gene of interest ORF (37). These final deletion constructs had the following generic arrangement: pETduet-1::5'-flank_SpecPromoter_kanR_3'-flank and were subsequently digested from the plasmid using BamHI and NotI (NEB). The resultant insert (5'-flank_SpecPromoter_kanR_3'-flank) was gel extracted (Monarch DNA GEL Extraction Kit, NEB) and added to competence peptide stimulated *S. intermedii* cells (see above).

Secretion Assays. Culture tubes containing 2 mL THY broth were inoculated with *S. intermedii* colonies from THY agar plates and grown overnight (final OD₆₀₀ of 1.0–1.1). Overnight cultures were then back diluted 1:100 into fresh 20 mL THY and grown overnight for a second iteration. Cell and secreted (sec) fractions were then separated by centrifugation at 4,000 *g* for 15 min. The cell samples were washed once in 1 mL of PBS pH 7.4 and centrifuged at 4,000 *g* for 5 min. PBS wash was decanted, and the cell samples were resuspended in 150 µL of 1:1 ratio of PBS to 4× Laemmli buffer, after which the cell samples were boiled for 10 min. The decanted sec samples were treated with trichloroacetic acid to a 10% final volume and the samples were incubated at 4 °C overnight to precipitate secreted protein. The sec samples were then centrifuged at 35,000 *g* for 30 min and resulting pellets were washed once with 20 mL of 95% cold acetone. Sec samples were centrifuged again at 35,000 *g* for 30 min and the acetone was removed. The sec samples were allowed to air dry briefly on ice in a fume hood. The precipitated protein pellets were then resuspended in 100 µL of 1:2 ratio of 4× Laemmli buffer to 8M urea and boiled for 10 min. Cell and sec samples were analyzed for proteins of interest by SDS-PAGE and western blotting.

Nano-Luciferase Assay. Nano-luciferase (NanoLuc)-based secretion assay was performed as described by Yang and colleagues (25). In brief, 2 mL THY cultures were inoculated with *S. intermedii* colonies from a THY agar plate and grown overnight to an OD₆₀₀ of 1.0–1.1. Cultures were centrifuged at 4,000 *g* for 10 min and 100 µL of supernatant was aliquoted into a clear bottom, black-walled 96-well plate (Corning #3631). NanoLuc large subunit 11S was purified and added into the reaction well at a final concentration of 5 µM as per published protocol (38). Then, 2 µL furimazine substrate was added to the reaction well from a working reagent stock of a 2:100 NanoDLR Stop & Glo Substrate to Buffer ratio (Promega #N1610). A total well volume of approximately 112.5 µL was incubated at room temperature for 2 min prior to measuring luminescence and OD₆₀₀ readings on an EnVision plate reader (PerkinElmer).

Antibody Generation. A custom polyclonal antibody for TelA was generated for this study. Because full-length TelA toxin is toxic to *E. coli*, overexpression of just the LXG domain of TelA (TelA_{LXG}) was performed for antibody production (4). To improve TelA_{LXG} stability, we co-expressed and co-purified TelA_{LXG} with LapA4. This complex was purified in PBS pH 7.4 and yielded 10 mg of total protein that was subsequently shipped to Genscript for custom antibody production. The generation of the α-TelC antibody was described previously (4).

SDS-PAGE, SYPRO Red Staining, and Western Blotting. A tris-tricine buffering system (200 mM Tris, 100 mM Tricine, 0.1% SDS, pH 8.3) was used for all SDS-PAGE gels run in this study

to better differentiate proteins less than 30 kDa (39). In-gel imaging of proteins was done using SYPRO Red protein gel stain (Invitrogen). The gels were rinsed in deionized water, stained in 1:5,000 SYPRO red, 10% acetic acid for 1 h, destained in 7.5% acetic acid for 1 min and imaged using a ChemiDoc imaging system (Bio-Rad). For western blotting, gels were wet transferred to nitrocellulose at 100 V for 30 min (α -TelC and α -V short for α -VSV-G) or to methanol-activated PVDF at 80 V for 1 h (α -EsxA). The blots were blocked with 5% skim milk in TBS-T for 30 min before being incubated with primary antibody for 1 h (1:5,000 titer for α -TelC and α -EsxA, and 1:3,000 titer for α -V). Blots were washed three times with 15 mL TBS-T and then incubated with α -rabbit secondary antibody (1:5,000 titer) for 45 min. Blots were washed three more times in TBS-T before being developed with Clarity Max Western ECL reagent and imaged on a ChemiDoc XRS+ (Bio-Rad).

Protein Expression and Purification. Wild-type and mutant TelA_{LXG}-LapA3-LapA4 protein complexes were expressed in BL21 (DE3) CodonPlus. The strains were back diluted 1:50 in LB supplemented with 50 μ L/mL of kanamycin and 150 μ L/mL of carbenicillin and grown to an OD₆₀₀ 0.50–0.55. Protein expression was then induced by the addition of 1 mM IPTG and protein was expressed overnight (~18 h) at 18 °C. The cells were pelleted, resuspended in lysis buffer (20 mM Tris-HCl pH 8.0, 300 mM NaCl, 10 mM imidazole), and sonicated four times for 30 s at 30% amplitude. Cellular debris was cleared by 30 min of centrifugation at 35,000 *g*. The lysate sample was run on a benchtop Ni-NTA column and washed thrice with 20 mL of lysis buffer. Protein was eluted with 4 mL of elution buffer (20 mM Tris-HCl pH 8.0, 300 mM NaCl, 400 mM imidazole). For protein crystallization trials, the eluants were then further purified by size exclusion chromatography using a HiLoad 16/600 Superdex 200 or Superdex 200 Increase 10/300 GL columns hooked up to a ÄKTA explorer (Cytiva). A similar protocol was used for the purification of TelB_{LXG}-LapB3-LapB4 complex except that lysis and elution buffers were additionally supplemented with 1 mM dithiothreitol.

Protein Crystallization. Native TelA_{LXG}-LapA3-LapA4 complex at 10 mg/mL was screened for crystallization conditions using the hanging drop vapor diffusion method and the MCSG suite of sparse matrix crystal screens (Anatrace). Crystals formed after 1 to 2 wk in 0.02M MgCl₂, 0.1M HEPES:NaOH pH 7.5, and 22% (w/v) polyacrylic acid 5100. The crystals were cryoprotected using the same buffer supplemented with 25% ethylene glycol and flash-frozen in liquid nitrogen prior to X-ray data collection.

Protein Structure Prediction, Visualization, and Analysis. Protein secondary structure predictions were generated by PSIPRED 4.0 on the UCL PSIPRED Workbench at hyperlink: <http://bioinf.cs.ucl.ac.uk/psipred/> (40). Protein complex predictions were performed with Colabfold AlphaFold2 using MMseqs2 locally installed on an HPE Apollo 6500 system running Red Hat Enterprise Linux with Nvidia Quadro RTX 8000 GPUs (41, 42). Predicted models were manually assessed and selected based on the per-residue pLDDT scores for each chain and the biological plausibility of the predicted complex. UCSF ChimeraX was used for protein structure analysis and figure generation (43). Surface hydrophobicity calculations were performed using default parameters (44). Interchain interfaces were analyzed using PDBsum (45). All structural alignments and reported RMSD scores were calculated by the DALI webserver using PDB search and Pairwise alignment tools (46).

X-ray Data Collection, Structure Determination, and Model Refinement. Data collection was performed using the Structural Biology Center sector 19-ID beamline at the Advanced Photon Source. Diffraction data were collected at 100K with 0.3 s exposure and a 0.5 degree of rotation for a total of 400 degrees. The crystal used to solve the structure diffracted to 2.6 Å and diffraction images were collected on a Dectris Pilatus 3 X 6M detector using an X-ray wavelength of 12.662 keV (0.97918 Å). Diffraction data were processed using HKL3000 software and the structure of TelA_{LXG}-LapA3-LapA4 was solved by molecular replacement using MOLREP implemented in HKL3000 with an AlphaFold2 generated model of the trimeric complex as a search model (47, 48). Coot was used to adjust the model manually to the electron density while computational structural refinement was performed with Phenix.refine until the R_{work} and R_{free} converged to 21.5% and 25.8%, respectively (49, 50). The final model includes two copies of each protein in the unit cell of space group P1. All collection and refinement statistics for TelA_{LXG}-LapA3-LapA4 can be found in Table 1 and the structure is deposited in the Protein Data Bank under PDB code 8GMH.

Sequence Analysis and Sequence Logo Generation. Homologous sequences to LapA3, LapA4, and TelA_{LXG} were identified using JackHMMER (HmmerWeb v2.41.2) searches of the UniprotKB database, restricted to the phylum Firmicutes, iterating until at least 150 sequences were obtained (51). Accessions were downloaded and full sequences of active entries were subsequently retrieved from Uniprot. Duplicate sequences were removed and the remaining aligned using ClustalO with default parameters (52). HMMs for each sequence alignment were generated using the Skylign webserver, set to “create HMM—remove mostly empty columns” (53). The resulting matrices were downloaded as tabular text, formatted and then visualized using Logomaker (54).

SEC-MALS Analysis of Protein Complexes. Size exclusion chromatography (SEC) with multi-angle laser light scattering (MALS) was performed on TelA_{LXG}-LapA3-LapA4 and TelB_{LXG}-LapB3-LapB4 protein complexes. The proteins were expressed and purified as described above and concentrated to 2 mg/mL by spin filtration. SEC was run on a Superdex 200 column (GE Healthcare), and MALS was conducted using a MiniDAWN and Optilab system (Wyatt Technologies). Data were collected and analyzed using the Astra software package (Wyatt Technologies).

Circular Dichroism Spectroscopy. Circular dichroism spectroscopy was performed on wild-type TelA_{LXG}-LapA3-LapA4 complex and variant complexes containing each of the following point mutations: TelA_{L41Q}, LapA3_{D79A}, or LapA3_{D80A}. The proteins were expressed and purified as described above and concentrated to 0.1 mg/mL by spin filtration. Circular dichroism spectroscopy was performed on a JASCO J-1100 instrument and data were collected and analyzed using the CDPro software package (JASCO).

Data, Materials, and Software Availability. The X-ray structure factors for the TelA_{LXG}-LapA3-LapA4 complex have been deposited in the Protein Data Bank under the accession number 8GMH (55).

ACKNOWLEDGMENTS. We thank Tracy Palmer for sharing protocols and reagents, Giuseppe Melacini and Madoka Akimoto for access to and training on the SEC-MALS system, Dana Sowa for assistance with circular dichroism spectroscopy, and members of the Whitney Lab for helpful discussions. We sincerely thank the members of the Structural Biology Center (SBC) at Argonne National Laboratory for their help with data collection at the 19-ID beamline. The use of SBC beamlines at the Advanced Photon Source is supported by the U.S. Department of Energy (DOE) Office of Science and operated for the DOE Office of Science by Argonne

National Laboratory under contract no. DE-AC02-06CH11357. T.A.K. and P.Y.S. are supported by Canada Graduate Scholarships from the Natural Sciences and Engineering Research Council of Canada. This work was supported by a project

grant (PJT-173486) from the Canadian Institutes of Health Research. J.C.W. is the Canada Research Chair in Molecular Microbiology and holds an Investigators in the Pathogenesis of Infectious Disease Award from the Burroughs Wellcome Fund.

1. H. R. Tran, D. W. Grebenc, T. A. Klein, J. C. Whitney, Bacterial type VII secretion: An important player in host-microbe and microbe-microbe interactions. *Mol. Microbiol.* **115**, 478–489 (2021).
2. A. M. Abdallah *et al.*, Type VII secretion-mycobacteria show the way. *Nat. Rev. Microbiol.* **5**, 883–891 (2007).
3. Z. Cao, M. G. Casabona, H. Kneuper, J. D. Chalmers, T. Palmer, The type VII secretion system of *Staphylococcus aureus* secretes a nuclease toxin that targets competitor bacteria. *Nat. Microbiol.* **2**, 16183 (2016).
4. J. C. Whitney *et al.*, A broadly distributed toxin family mediates contact-dependent antagonism between gram-positive bacteria. *ELife* **6**, e26938 (2017).
5. K. Kobayashi, Diverse LXG toxin and antitoxin systems specifically mediate intraspecies competition in *Bacillus subtilis* biofilms. *PLoS Genet.* **17**, e1009682 (2021).
6. A. Chatterjee, J. L. E. Willett, G. M. Dunny, B. A. Duerkop, Phage infection and sub-lethal antibiotic exposure mediate *Enterococcus faecalis* type VII secretion system dependent inhibition of bystander bacteria. *PLoS Genet.* **17**, e1009204 (2021).
7. M. L. Burts, W. A. Williams, K. DeBord, D. M. Missiakos, EsxA and EsxB are secreted by an ESAT-6-like system that is required for the pathogenesis of *Staphylococcus aureus* infections. *Proc. Natl. Acad. Sci. U.S.A.* **102**, 1169–1174 (2005).
8. L. Bowman, T. Palmer, The type VII secretion system of *Staphylococcus*. *Ann. Rev. Microbiol.* **75**, 471–494 (2021).
9. T. A. Sysoeva, M. A. Zepeda-Rivera, L. A. Huppert, B. M. Burton, Dimer recognition and secretion by the ESX secretion system in *Bacillus subtilis*. *Proc. Natl. Acad. Sci. U.S.A.* **111**, 7653–7658 (2014).
10. D. Zhang, R. F. de Souza, V. Anantharaman, L. M. Iyer, L. Aravind, Polymorphic toxin systems: Comprehensive characterization of trafficking modes, processing, mechanisms of action, immunity and ecology using comparative genomics. *Biol. Direct* **7**, 18 (2012).
11. F. R. Ulhuq *et al.*, A membrane-depolarizing toxin substrate of the *Staphylococcus aureus* type VII secretion system mediates intraspecies competition. *Proc. Natl. Acad. Sci. U.S.A.* **117**, 20836–20847 (2020), 10.1073/pnas.2006110117.
12. T. A. Klein *et al.*, Dual targeting factors are required for LXG toxin export by the bacterial type VIIb secretion system. *mBio* **13**, e0213722 (2022), 10.1128/mbio.02137-22.
13. M. H. Daleke *et al.*, General secretion signal for the mycobacterial type VII secretion pathway. *Proc. Natl. Acad. Sci. U.S.A.* **109**, 11342–11347 (2012).
14. M. Solomonson *et al.*, Structure of EspB from the ESX-1 type VII secretion system and insights into its export mechanism. *Structure* **23**, 571–583 (2015).
15. W. K. Teh *et al.*, Characterization of TeLE, a T7SS LXG effector exhibiting a conserved C-terminal glycine zipper motif required for toxicity. *Microbiol. Spectr.* **11**, e0148123 (2023), 10.1128/spectrum.01481-23.
16. O. S. Rosenberg *et al.*, Substrates control multimerization and activation of the multi-domain ATPase motor of type VII secretion. *Cell* **161**, 501–512 (2015).
17. N. Famelis *et al.*, Architecture of the mycobacterial type VII secretion system. *Nature* **576**, 321–325 (2019).
18. C. M. Bunduc *et al.*, Structure and dynamics of a mycobacterial type VII secretion system. *Nature* **593**, 445–448 (2021).
19. P. A. Karplus, K. Diederichs, Linking crystallographic model and data quality. *Science* **336**, 1030–1033 (2012).
20. I. W. Davis, L. W. Murray, J. S. Richardson, D. C. Richardson, MOLPROBITY: Structure validation and all-atom contact analysis for nucleic acids and their complexes. *Nucleic Acids Res.* **32**, W615–W619 (2004).
21. N. Korotkova *et al.*, Structure of the *Mycobacterium tuberculosis* type VII secretion system chaperone EspG5 in complex with PE25-PPE41 dimer. *Mol. Microbiol.* **94**, 367–382 (2014).
22. J. Piton, F. Pojer, S. Wakatsuki, C. Gati, S. T. Cole, High resolution CryoEM structure of the ring-shaped virulence factor EspB from *Mycobacterium tuberculosis*. *J. Struct. Biol. X* **4**, 100029 (2020).
23. Q. Wang *et al.*, PE/PPE proteins mediate nutrient transport across the outer membrane of *Mycobacterium tuberculosis*. *Science* **367**, 1147–1151 (2020).
24. Y. Lou, J. Rybniker, C. Sala, S. T. Cole, EspC forms a filamentous structure in the cell envelope of *Mycobacterium tuberculosis* and impacts ESX-1 secretion. *Mol. Microbiol.* **103**, 26–38 (2017).
25. Y. Yang, F. Alcock, H. Kneuper, T. Palmer, A high throughput assay to measure Type VII secretion in *Staphylococcus aureus*. *bioRxiv [Preprint]* (2023). <https://doi.org/10.1101/2023.06.03.543475> (Accessed 1 July 2023).
26. T. A. Klein, M. Pazos, M. G. Surette, W. Vollmer, J. C. Whitney, Molecular basis for immunity protein recognition of a type VII secretion system exported antibacterial toxin. *J. Mol. Biol.* **430**, 4344–4358 (2018).
27. Y. Yang *et al.*, Three small partner proteins facilitate the type VII-dependent secretion of an antibacterial nuclease. *mBio* **14**, e0210023 (2023), 10.1128/mbio.02100-23.
28. M. H. Daleke *et al.*, Specific chaperones for the type VII protein secretion pathway. *J. Biol. Chem.* **287**, 31939–31947 (2012).
29. M. Zoltner *et al.*, EssC: Domain structures inform on the elusive translocation channel in the Type VII secretion system. *Biochem. J.* **473**, 1941–1952 (2016).
30. N. Powelleit *et al.*, The structure of the endogenous ESX-3 secretion system. *ELife* **8**, e52983 (2019).
31. B. Warne *et al.*, The Ess/Type VII secretion system of *Staphylococcus aureus* shows unexpected genetic diversity. *BMC Genomics* **17**, 222 (2016).
32. F. Jager, H. Kneuper, T. Palmer, EssC is a specificity determinant for *Staphylococcus aureus* type VII secretion. *Microbiol. (Reading)* **164**, 816–820 (2018).
33. K. Bowman, T. Palmer, Extreme genetic diversity in the type VII secretion system of *Listeria monocytogenes* suggests a role in bacterial antagonism. *Microbiol. (Reading)* **167**, mic.0.001034 (2021).
34. M. Lo Sapio, M. Hilleringmann, M. A. Barocchi, M. Moschioni, A novel strategy to over-express and purify homologous proteins from *Streptococcus pneumoniae*. *J. Biotechnol.* **157**, 279–286 (2012).
35. T. Tomoyasu *et al.*, Role of catabolite control protein A in the regulation of intermedilysin production by *Streptococcus intermedius*. *Infect. Immunity* **78**, 4012–4021 (2010).
36. T. A. Klein *et al.*, Structure of the extracellular region of the bacterial type VIIb secretion system subunit EsaA. *Structure* **29**, 177–185.e6 (2020), 10.1016/j.str.2020.11.002.
37. A. V. Bryksin, I. Matsumura, Rational design of a plasmid origin that replicates efficiently in both gram-positive and gram-negative bacteria. *PLoS one* **5**, e13244 (2010).
38. G. C. Pereira *et al.*, A high-resolution luminescent assay for rapid and continuous monitoring of protein translocation across biological membranes. *J. Mol. Biol.* **431**, 1689–1699 (2019).
39. H. Schagger, Tricine-SDS-PAGE. *Nat. Protoc.* **1**, 16–22 (2006).
40. D. W. A. Buchan, D. T. Jones, The PSIPRED protein analysis workbench: 20 years on. *Nucleic Acids Res.* **47**, W402–W407 (2019).
41. J. Jumper *et al.*, Highly accurate protein structure prediction with AlphaFold. *Nature* **596**, 583–589 (2021).
42. M. Mirdita *et al.*, ColabFold: Making protein folding accessible to all. *Nat. Methods* **19**, 679–682 (2022).
43. T. D. Goddard *et al.*, UCSF ChimeraX: Meeting modern challenges in visualization and analysis. *Protein Sci.* **27**, 14–25 (2018).
44. B. Testa, P. A. Carrupt, P. Gaillard, F. Billois, P. Weber, Lipophilicity in molecular modeling. *Pharm. Res.* **13**, 335–343 (1996).
45. R. A. Laskowski, PDBsum: Summaries and analyses of PDB structures. *Nucleic Acids Res.* **29**, 221–222 (2001).
46. L. Holm, Using Dali for protein structure comparison. *Methods Mol. Biol.* **2112**, 29–42 (2020).
47. W. Minor, M. Cymborowski, Z. Otwinowski, M. Chruszcz, HKL-3000: The integration of data reduction and structure solution—from diffraction images to an initial model in minutes. *Acta Crystallogr. D Biol. Crystallogr.* **62**, 859–866 (2006).
48. A. Vagin, A. Teplyakov, Molecular replacement with MOLREP. *Acta Crystallogr. D Biol. Crystallogr.* **66**, 22–25 (2010).
49. P. Emsley, B. Lohkamp, W. G. Scott, K. Cowtan, Features and development of Coot. *Acta Crystallogr. D Biol. Crystallogr.* **66**, 486–501 (2010).
50. P. V. Afonine *et al.*, Towards automated crystallographic structure refinement with phenix.refine. *Acta Crystallogr. D Biol. Crystallogr.* **68**, 352–367 (2012).
51. R. D. Finn *et al.*, HMMER web server: 2015 update. *Nucleic Acids Res.* **43**, W30–W38 (2015).
52. F. Sievers *et al.*, Fast, scalable generation of high-quality protein multiple sequence alignments using Clustal Omega. *Mol. Syst. Biol.* **7**, 539 (2011).
53. T. J. Wheeler, J. Clements, R. D. Finn, Skyline: A tool for creating informative, interactive logos representing sequence alignments and profile hidden Markov models. *BMC Bioinformatics* **15**, 7 (2014).
54. A. Tareen, J. B. Kinney, Logomaker: Beautiful sequence logos in Python. *Bioinformatics* **36**, 2272–2274 (2020).
55. T. A. Klein *et al.*, Crystal Structure of the ternary complex of TeLA-LXG, LapA3, and LapA4. Protein Data Bank (PDB). 10.2210/pdb8gmh/pdb. Deposited 25 March 2023.